ELSEVIER

Nuclear Instruments and Methods in Physics Research A 404 (1998) 129–142

NUCLEAR INSTRUMENTS & METHODS IN PHYSICS RESEARCH Section A

Analyzing powers for the inclusive reaction of deuterons on carbon at energies between 0.175 and 1.6 GeV

V.P. Ladygin[a,f], E. Tomasi-Gustafsson[a,b,*], J. Ball[a,b], L. Bimbot[c], Y. Bisson[c], M. Boivin[a], J.L. Boyard[c], N.E. Cheung[d], Ph. Courtat[c], R. Gacougnolle[e], T. Hennino[c], M.K. Jones[e], R.A. Kunne[a], C.F. Perdrisat[d], N.M. Piskunov[f], V. Punjabi[e], I.M. Sitnik[f], R. Skowron[c], E.A. Strokovsky[f], P. Zupranski[g]

[a] *CEA/DSM CNRS/IN2P3 Laboratoire National Saturne, CE Saclay, F-91191-Gif-sur-Yvette, France*
[b] *CEA/DSM DAPNIA-SPhN, CE Saclay, F-91191-Gif-sur-Yvette, France*
[c] *CNRS/IN2P3 IPN, 91400 Orsay, France*
[d] *The College of William and Mary, Williamsburg, VA 23187, USA*
[e] *Norfolk State University, Norfolk, VA 23504, USA*
[f] *JINR-LHE, 141980 Dubna, Moscow region, Russian Federation*
[g] *Soltan Institute for Nuclear Studies, 00-681 Warsaw, Poland*

Received 23 September 1997

Abstract

The results of a new calibration of the polarimeter POMME for energies between 0.175 and 1.6 GeV, using the polarized deuteron beam of the Laboratoire National Saturne, are reported. The present calibration, together with previous ones, gives a complete set of vector analyzing powers in the energy range 0.175–1.8 GeV. The vector analyzing powers are fitted as a function of energy and scattering angle, with empirical formulae. Two sets of parameters are given, one for deuteron energies between 0.175 and 0.575 GeV, and the other in an energy range between 0.7 and 1.8 GeV.

1. Introduction

Many studies in intermediate energy physics require measurement of the polarization of the secondary particles of a reaction. These investigations provide stringent tests of nuclear structure and reaction mechanism theories. The focal-plane polarimeter POMME with 2π azimuthal angular acceptance, based on inclusive scattering on a carbon target, was built for such a purpose. In the last few years POMME was used in a number of experiments at SATURNE as a deuteron polarimeter. One application has been the study of the isoscalar spin transitions in nuclei for low-lying levels, as well as in the continuum by inelastic $(\vec{d}, \vec{d}')$ scattering on nuclei [1,2]; another has been the measurement of the polarization of the deuteron in the reaction $\vec{p}p \to \vec{d}\pi^+$ [3].

* Corresponding author. E-mail: tomasi@republique.saclay.cea.fr.

0168-9002/98/$19.00
PII S0168-9002(97)01135-2

POMME was initially calibrated for deuteron energies up to 0.7 GeV [4]. In Ref. [4] an iron absorber and trigger counters behind the coordinate detectors were used to stop protons from the deuteron breakup in the carbon. The use of the iron absorber increases the analyzing power as the breakup reaction, which has small analyzing powers, is suppressed. We will show in the present work that this technique does not work at energies higher than 0.7 GeV because the stopping-power difference in iron for protons and deuterons is too small.

In a previous paper [5] the results of a calibration of POMME at 1.8 GeV with both carbon and paraffin targets were reported. These measurements were made without iron absorber and scintillator counters behind the chambers, in the same way as calibration for protons [6,7]. It was found in Ref. [5] that the vector analyzing powers and corresponding figures of merit are large even at this energy and can be used for polarimetry.

We report here new calibration results of POMME with polarized deuteron beam with energies from 0.175 to 0.300 and from 0.7 to 1.6 GeV. In the next section the polarimeter POMME is described briefly; in Section 3 the details of the calibration and data analysis are presented. Experimental results are given in Section 4 and fits at low energy and at high energy of deuteron–carbon data are described in Section 5. The conclusions are in the last section.

2. The polarimeter POMME

A detailed description of the polarimeter POMME is given in Refs. [4,6]. Here we briefly mention its main characteristics. In the polarimeter POMME the 2π azimuthal distribution of particles from the inclusive reaction $d + C \rightarrow$ *one charged particle* $+ X$ is measured. The layout of the polarimeter is shown in Fig. 1. Three front-proportional wire chambers with size $50 \times 50\ cm^2$ are used to determine the trajectories of the deuterons

Table 1
The optimum thicknesses of carbon and iron for the low-energy calibration

T_d (MeV)	Graphite (cm)	Iron (cm)
175	2.8	0.8
200	3.6	1.3
225	4.8	1.0
250	4.8	1.4
275	4.8	1.8
300	4.8	2.0

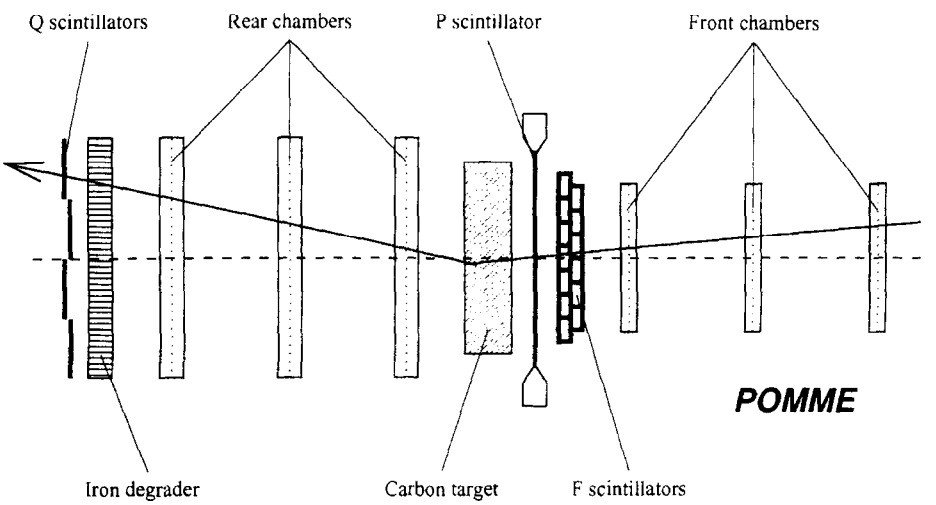

Fig. 1. Layout of polarimeter POMME.

incident on the carbon analyzer. The scattered particles are detected in three rear chambers which have dimension of $100 \times 100\ \mathrm{cm}^2$. Their resolution is approximately 1.7 and 3.2 mm for front and rear chambers, respectively. The chambers were mechanically aligned within 1 mm; however particle trajectories were used to obtain an alignment at the level of 0.1 mm, with a software procedure. A total thickness of 30 cm of graphite with a density of $1.7\mathrm{g/cm}^3$ was used as analyzer at energies between 0.7 and 1.6 GeV. Thicknesses of graphite and iron used for lower energies between 0.175 and 0.300 GeV are given in Table 1.

The trigger of the polarimeter is defined by a set of overlapping scintillators F_i placed close to the focal plane in coincidence with the counter P, and located just before the analyzer, covering the full size of the front chambers in the dispersive direction. The plane of scintillators Q placed behind the iron absorber, was part of the trigger for the low-energy calibration, but not for the high-energy measurement. No fast rejection of events with small scattering angles due to Coulomb interaction was done at the trigger level.

3. Experiment and data analysis

The polarimeter was calibrated using the polarized deuteron beam of the Laboratoire National Saturne, in the focal plane of the spectrometer SPES4 [8]. The polarized deuteron beam was directly incident on the polarimeter. The lowest intensity from the machine, $\simeq 10^8$ particles per beam burst, was further reduced to $\simeq 10^4 - 2 \times 10^4$ with the help of beam slits and by defocalizing the beam with the last quadrupoles of the line.

The polarized deuteron beam of Saturne has vector and tensor polarization components ρ_{10} and ρ_{20} along the vertical symmetry axis [9]. Different radiofrequency transitions in the ion source are combined to obtain either two states (only vector polarized), or four states of polarization (vector and tensor polarized), changing the sign of the components at each beam burst. The polarization of the deuteron beam was measured in a low-energy polarimeter [9] located at the exit of the source. The measured values were very stable, and we used, in the analysis, averaged values over the whole duration of the calibration. With the four-state beam, the vector and tensor polarizations were $\rho_{10} = -0.40 \pm 0.02$ and $\rho_{20} = 0.65 \pm 0.02$, respectively. For the purely vector polarized beam, $\rho_{10} = 0.80 \pm 0.02$. During the calibration, we used beam with four states at energy 1.6 GeV, and two states of polarization at all other energies. The change of the polarization state at every beam burst cancels the instrumental asymmetries.

During the off-line analysis, the incoming and outgoing particle trajectories were reconstructed using the information from the multiwire proportional chambers. Next, the vertex of the reaction in the carbon and the polar and azimuthal scattering angles, θ and ϕ, were calculated. Vertex cuts, compatible with the location of the analyzer, as well as a cut on the distance between incoming and outgoing tracks, were required. A cone test, which requires that for an event with given polar-θ and azimuthal-ϕ angles, any other choice of ϕ would be within the large chambers, was applied to remove the instrumental asymmetry introduced by the finite size of the chambers downstream of the analyzer. Events which passed all tests were used to determine the analyzing power and efficiency of the polarimeter. For each spin state of the beam (s), a two-dimensional array of $N^{(s)}(\theta, \phi)$ was filled by the selected events, monitored on the beam intensity. The angular ranges were $0^\circ \leqslant \theta \leqslant 20^\circ$ and $-180^\circ \leqslant \phi \leqslant 180^\circ$, with bins of 1° and 10° for θ and ϕ, respectively.

In the general case with vertical symmetry axis of the deuteron polarization, the number of events in each (θ, ϕ) bin can be written as

$$N^{(s)}(\theta, \phi) = N_0(\theta)\left[1 + \sqrt{2}\rho_{10} i T_{11}(\theta)\cos\phi - \frac{1}{2}\rho_{20} T_{20}(\theta) - \sqrt{\frac{3}{2}}\rho_{20} T_{22}(\theta)\cos 2\phi\right], \quad (1)$$

where the T_{ij}'s are the analyzing powers and $N_0(\theta)$ is the average number of events per ϕ-bin.

Combinations of the events from $N^{(s)}(\theta, \phi)$ distributions with different polarization states

give either purely vector or purely tensor distributions:

$$R_V(\theta, \phi) = \frac{N^{(5)} + N^{(7)} - N^{(6)} - N^{(8)}}{N^{(5)} + N^{(7)} + N^{(6)} + N^{(8)}}$$

$$= \sqrt{2}\rho_{10} i T_{11}(\theta) \cos\phi = A_1(\theta) \cos\phi, \quad (2)$$

$$R_T(\theta, \phi) = \frac{N^{(5)} + N^{(6)} - N^{(7)} - N^{(8)}}{N^{(5)} + N^{(7)} + N^{(6)} + N^{(8)}}$$

$$= -\frac{1}{2}\rho_{20} T_{20}(\theta) - \sqrt{\frac{3}{2}}\rho_{20} T_{22}(\theta) \cos 2\phi$$

$$= A_0 + A_2(\theta) \cos 2\phi, \quad (3)$$

The vector analyzing power iT_{11} or tensor analyzing powers T_{20} and T_{22} are obtained by fitting these R_V and R_T distributions, respectively.

For a purely vector-polarized beam the vector ratio is defined as

$$R_V(\theta, \phi) = \frac{N^{(2)} - N^{(3)}}{N^{(2)} + N^{(3)}}. \quad (4)$$

4. Results

The performance of a polarimeter is usually expressed in terms of the figures of merit, $\mathscr{F}_{ij}$, where ij are the tensorial indices. These depend on the polar angle θ and are functions of the differential efficiency, $\varepsilon(\theta)$, and analyzing powers, $T_{ij}(\theta)$. The figures of merit are defined as

$$\mathscr{F}_{ij}^2 = \int_{\theta_{min}}^{\theta_{max}} \varepsilon(\theta)\, T_{ij}^2(\theta)\, d\theta = \int_{\theta_{min}}^{\theta_{max}} g_{ij}^2(\theta)\, d\theta, \quad (5)$$

where $g_{ij}(\theta)$ is the differential figure of merit and the integration is done over the angular range where the polarimeter is efficient. The differential efficiency $\varepsilon(\theta) = N_0(\theta)/N_{inc}$ is defined as the ratio between the number of events in a given θ-bin, and the number of events incident on the carbon analyzer. It depends on the differential cross section of the reaction and on the geometry and efficiency of the detection. The typical efficiency of the track reconstruction after the analyzer was between 60% and 80%, depending on the experimental conditions. Due to the high beam flux during the calibration, the efficiency of the large chambers is lower than during a normal operation as a polarimeter. In order to obtain a real value of the efficiency and figure of merit the values quoted in tables are corrected for 100% track reconstruction.

The overall polarimeter efficiency, ε, is then

$$\varepsilon = \int_{\theta_{min}}^{\theta_{max}} \varepsilon(\theta)\, d\theta. \quad (6)$$

The figures of merit F_{ij} are used to determine the number of events, N_{inc}, necessary to obtain a given statistical uncertainty, ΔT_{ij}, in a polarization measurement:

$$\Delta T_{ij} = \sqrt{\frac{2 - \delta_{j0}}{N_{inc}\, \mathscr{F}_{ij}^2}}, \quad (7)$$

where δ_{j0} is the Kronecker symbol (as an example, it is zero for the tensor-analyzing power T_{20} and one for the vector-analyzing power iT_{11}). All uncertainties shown in the next two subsections are statistical only. The main source of systematic error comes from the measurement of ρ_{10} and ρ_{20}, which were evaluated to be $\pm 2\%$. The errors caused by instrumental asymmetries are cancelled because distributions with opposite polarization are being subtracted as shown in Eq. (3) and (4). All results presented below were obtained with an incident beam of a few centimeters in the focal plane. In an experiment using the polarimeter to measure the polarization of deuterons emerging from a reaction at the primary target, and spread over the whole focal plane, efficiencies and figures of merit would be smaller due to events lost in the cone test.

4.1. Low-energy results

The results of the calibration for the vector-analyzing power iT_{11} at the six lower energies 0.175, 0.200, 0.225, 0.250, 0.275 and 0.300 GeV are given in Table 2(a) and are shown as a function of the polar angle in Fig. 2. As no fast small-angle rejection was available, the θ range is limited to $\theta_{min} \geqslant 3^\circ$ and $\theta_{max} \leqslant 15^\circ$. Table 2 (b) contains the values of the differential efficiency $\varepsilon(\theta)$ which are shown in Fig. 3.

Even though these data are restricted in polar-angle range, when combined with the previous data, they are helpful in constraining the parameters of the low-energy fit.

Table 2
(a) Analyzing powers $iT_{11}(\theta)$ for six lower energies; error bars are statistical only

θ (deg)	0.175 GeV	0.200 GeV	0.225 GeV	0.250 GeV	0.275 GeV	0.300 GeV
4	0.02 ± 0.01	0.05 ± 0.01	0.05 ± 0.01	0.08 ± 0.01	0.11 ± 0.01	0.12 ± 0.01
5	0.03 ± 0.01	0.04 ± 0.01	0.06 ± 0.01	0.08 ± 0.01	0.12 ± 0.01	0.14 ± 0.01
6	0.02 ± 0.01	0.05 ± 0.01	0.06 ± 0.01	0.10 ± 0.01	0.16 ± 0.01	0.19 ± 0.01
7	0.01 ± 0.01	0.05 ± 0.01	0.07 ± 0.01	0.10 ± 0.01	0.17 ± 0.01	0.21 ± 0.01
8	0.01 ± 0.01	0.06 ± 0.01	0.08 ± 0.01	0.13 ± 0.01	0.18 ± 0.01	0.23 ± 0.01
9	0.01 ± 0.01	0.06 ± 0.01	0.08 ± 0.01	0.15 ± 0.01	0.22 ± 0.01	0.28 ± 0.01
10	0.00 ± 0.01	0.07 ± 0.02	0.11 ± 0.01	0.18 ± 0.01	0.25 ± 0.01	0.27 ± 0.01
11	0.00 ± 0.01	0.11 ± 0.02	0.13 ± 0.01	0.19 ± 0.02	0.25 ± 0.01	0.25 ± 0.01
12	0.03 ± 0.02	0.12 ± 0.02	0.16 ± 0.02	0.25 ± 0.02	0.26 ± 0.02	0.24 ± 0.02
13	0.07 ± 0.02	0.13 ± 0.04	0.11 ± 0.02	0.17 ± 0.03	0.27 ± 0.02	0.20 ± 0.02
14	0.07 ± 0.04			0.24 ± 0.08	0.11 ± 0.01	0.21 ± 0.02
15	0.16 ± 0.04				0.18 ± 0.05	

(b) Efficiencies $\varepsilon(\theta)$ for six lower energies; error bars are statistical only

θ (deg)	0.175 GeV	0.200 GeV	0.225 GeV
4	$(1.88 \pm 0.01)10^{-2}$	$(7.30 \pm 0.04)10^{-3}$	$(1.05 \pm 0.01)10^{-2}$
5	$(1.00 \pm 0.01)10^{-2}$	$(8.12 \pm 0.04)10^{-3}$	$(1.14 \pm 0.01)10^{-2}$
6	$(1.04 \pm 0.01)10^{-2}$	$(8.39 \pm 0.04)10^{-3}$	$(1.17 \pm 0.01)10^{-2}$
7	$(1.03 \pm 0.05)10^{-2}$	$(7.57 \pm 0.04)10^{-3}$	$(1.04 \pm 0.01)10^{-2}$
8	$(9.32 \pm 0.05)10^{-3}$	$(6.19 \pm 0.034)10^{-3}$	$(8.43 \pm 0.04)10^{-3}$
9	$(7.81 \pm 0.04)10^{-3}$	$(4.51 \pm 0.033)10^{-3}$	$(6.34 \pm 0.04)10^{-3}$
10	$(6.11 \pm 0.04)10^{-3}$	$(3.07 \pm 0.027)10^{-3}$	$(4.48 \pm 0.03)10^{-3}$
11	$(4.42 \pm 0.03)10^{-3}$	$(1.86 \pm 0.02)10^{-3}$	$(2.74 \pm 0.02)10^{-3}$
12	$(2.94 \pm 0.03)10^{-3}$	$(8.67 \pm 0.14)10^{-4}$	$(1.20 \pm 0.02)10^{-3}$
13	$(1.68 \pm 0.03)10^{-3}$	$(2.83 \pm 0.08)10^{-4}$	$(3.44 \pm 0.01)10^{-4}$
14	$(8.37 \pm 0.14)10^{-4}$	$(0.40 \pm 0.03)10^{-4}$	
15	$(2.56 \pm 0.07)10^{-4}$		

θ (deg)	0.250 GeV	0.275 GeV	0.300 GeV
4	$(9.61 \pm 0.05)10^{-3}$	$(9.43 \pm 0.04)10^{-3}$	$(1.00 \pm 0.01)10^{-2}$
5	$(1.31 \pm 0.01)10^{-2}$	$(1.00 \pm 0.01)10^{-2}$	$(1.03 \pm 0.01)10^{-2}$
6	$(1.11 \pm 0.01)10^{-2}$	$(9.09 \pm 0.04)10^{-3}$	$(8.89 \pm 0.01)10^{-3}$
7	$(1.01 \pm 0.01)10^{-2}$	$(7.18 \pm 0.04)10^{-3}$	$(6.82 \pm 0.01)10^{-3}$
8	$(9.06 \pm 0.09)10^{-3}$	$(5.23 \pm 0.03)10^{-3}$	$(4.83 \pm 0.01)10^{-3}$
9	$(8.50 \pm 0.09)10^{-2}$	$(3.67 \pm 0.03)10^{-3}$	$(3.40 \pm 0.03)10^{-3}$
10	$(7.92 \pm 0.09)10^{-3}$	$(2.52 \pm 0.02)10^{-3}$	$(2.41 \pm 0.02)10^{-3}$
11	$(7.59 \pm 0.09)10^{-2}$	$(1.77 \pm 0.02)10^{-3}$	$(1.81 \pm 0.02)10^{-3}$
12	$(7.02 \pm 0.09)10^{-3}$	$(1.23 \pm 0.01)10^{-3}$	$(1.41 \pm 0.02)10^{-3}$
13	$(6.96 \pm 0.09)10^{-3}$	$(0.63 \pm 0.01)10^{-3}$	$(9.99 \pm 0.01)10^{-4}$
14	$(6.52 \pm 0.08)10^{-3}$	$(2.06 \pm 0.06)10^{-4}$	$(5.27 \pm 0.11)10^{-4}$
15		$(1.91 \pm 0.01)10^{-2}$	$(1.47 \pm 0.06)10^{-4}$

4.2. High-energy results

The vector-analyzing powers iT_{11} at the four higher energies 0.700, 1.10, 1.35 and 1.60 GeV are shown as a function of the polar angle in Fig. 4 and are given in Table 3(a). The differential efficiencies, $\varepsilon(\theta)$, which are shown in Fig. 5, are listed in Table 3 (b). All these data were obtained with purely vector-polarized deuteron beam (two states).

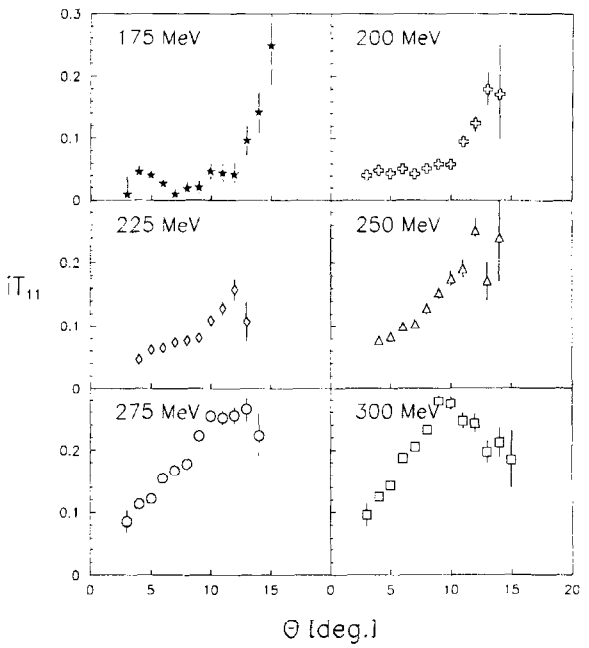

Fig. 2. Vector analyzing powers iT_{11} for the six lower energies.

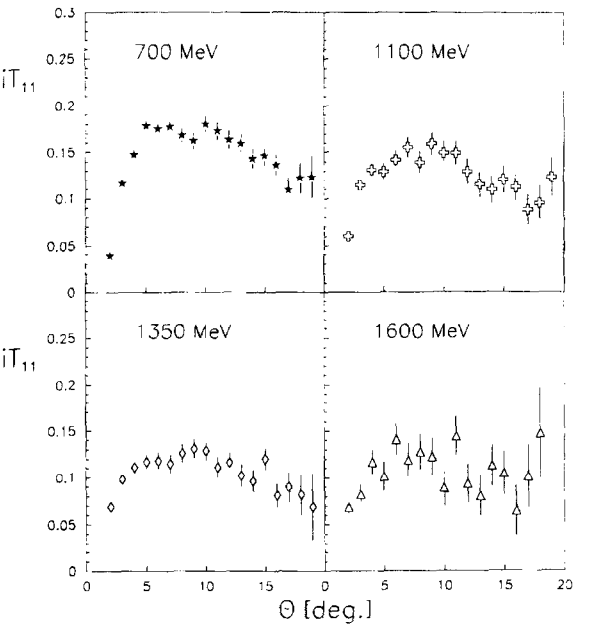

Fig. 4. Vector analyzing powers iT_{11} for the four higher energies.

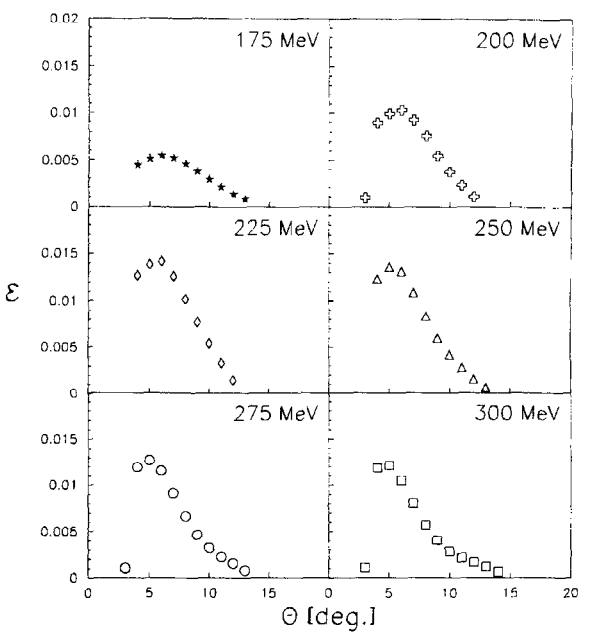

Fig. 3. Efficiency of the polarimeter at the same six energies as in Fig. 2, corrected for the track reconstruction efficiency.

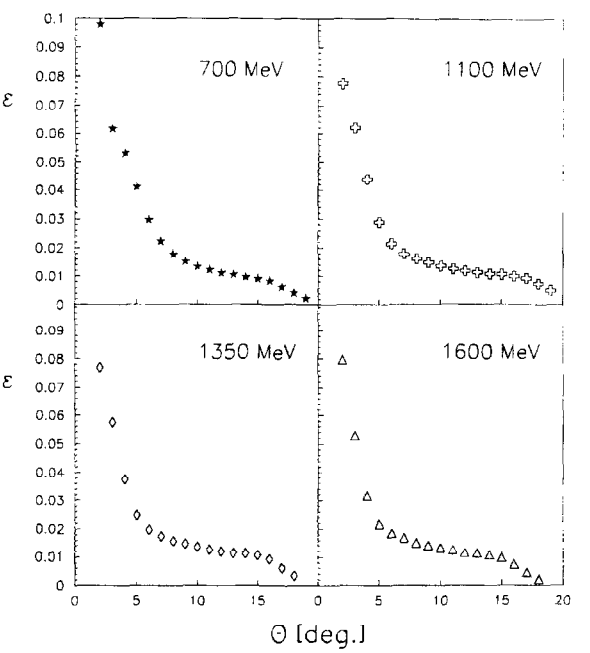

Fig. 5. Efficiency of the polarimeter at the four higher energies, corrected for 100% track reconstruction.

Table 3
(a) Analyzing powers $iT_{11}(\theta)$ for the four higher energies; error bars are statistical only

θ (deg)	0.7 GeV	1.1 GeV	1.35 GeV	1.6 GeV
2	0.04 ± 0.01	0.06 ± 0.01	0.07 ± 0.01	0.07 ± 0.01
3	0.12 ± 0.01	0.11 ± 0.01	0.10 ± 0.01	0.08 ± 0.01
4	0.15 ± 0.01	0.13 ± 0.01	0.11 ± 0.01	0.12 ± 0.01
5	0.18 ± 0.01	0.13 ± 0.01	0.12 ± 0.01	0.10 ± 0.02
6	0.18 ± 0.01	0.14 ± 0.01	0.12 ± 0.01	0.14 ± 0.02
7	0.18 ± 0.01	0.16 ± 0.01	0.12 ± 0.01	0.12 ± 0.02
8	0.17 ± 0.01	0.14 ± 0.01	0.13 ± 0.01	0.13 ± 0.02
9	0.16 ± 0.01	0.16 ± 0.01	0.13 ± 0.01	0.12 ± 0.02
10	0.18 ± 0.01	0.15 ± 0.01	0.13 ± 0.01	0.09 ± 0.02
11	0.17 ± 0.01	0.15 ± 0.01	0.11 ± 0.01	0.14 ± 0.02
12	0.16 ± 0.01	0.13 ± 0.01	0.12 ± 0.01	0.09 ± 0.02
13	0.16 ± 0.01	0.12 ± 0.01	0.10 ± 0.01	0.08 ± 0.02
14	0.14 ± 0.01	0.11 ± 0.02	0.10 ± 0.01	0.11 ± 0.02
15	0.15 ± 0.01	0.12 ± 0.02	0.12 ± 0.01	0.10 ± 0.02
16	0.14 ± 0.01	0.11 ± 0.02	0.08 ± 0.01	0.07 ± 0.03
17	0.10 ± 0.01	0.09 ± 0.02	0.09 ± 0.02	0.10 ± 0.04
18	0.12 ± 0.02	0.10 ± 0.02	0.08 ± 0.02	0.15 ± 0.05
19	0.12 ± 0.02	0.13 ± 0.02	0.07 ± 0.04	
20	0.14 ± 0.04	0.09 ± 0.03		

(b) Efficiencies $\varepsilon(\theta)$ for the four higher energies; error bars are statistical only

θ (deg)	0.7 GeV	1.1 GeV	1.35 GeV	1.6 GeV
2	$(3.47 \pm 0.01)10^{-2}$	$(4.58 \pm 0.02)10^{-2}$	$(3.54 \pm 0.01)10^{-2}$	$(4.82 \pm 0.02)10^{-2}$
3	$(2.18 \pm 0.01)10^{-2}$	$(3.66 \pm 0.02)10^{-2}$	$(2.64 \pm 0.01)10^{-2}$	$(3.20 \pm 0.02)10^{-2}$
4	$(1.88 \pm 0.01)10^{-2}$	$(2.59 \pm 0.02)10^{-2}$	$(1.72 \pm 0.01)10^{-2}$	$(1.91 \pm 0.01)10^{-2}$
5	$(1.45 \pm 0.01)10^{-2}$	$(1.71 \pm 0.01)10^{-2}$	$(1.14 \pm 0.01)10^{-2}$	$(1.31 \pm 0.01)10^{-2}$
6	$(1.05 \pm 0.01)10^{-2}$	$(1.26 \pm 0.01)10^{-2}$	$(9.10 \pm 0.06)10^{-3}$	$(1.11 \pm 0.01)10^{-2}$
7	$(7.88 \pm 0.05)10^{-3}$	$(1.05 \pm 0.01)10^{-2}$	$(8.01 \pm 0.06)10^{-3}$	$(1.01 \pm 0.01)10^{-2}$
8	$(6.28 \pm 0.04)10^{-3}$	$(9.53 \pm 0.09)10^{-3}$	$(7.24 \pm 0.06)10^{-3}$	$(9.06 \pm 0.09)10^{-3}$
9	$(5.33 \pm 0.01)10^{-3}$	$(8.76 \pm 0.09)10^{-3}$	$(6.79 \pm 0.06)10^{-3}$	$(8.50 \pm 0.09)10^{-3}$
10	$(4.70 \pm 0.04)10^{-3}$	$(8.00 \pm 0.08)10^{-3}$	$(6.25 \pm 0.05)10^{-3}$	$(7.92 \pm 0.09)10^{-3}$
11	$(4.34 \pm 0.03)10^{-3}$	$(7.39 \pm 0.08)10^{-3}$	$(5.84 \pm 0.05)10^{-3}$	$(7.59 \pm 0.09)10^{-3}$
12	$(3.92 \pm 0.03)10^{-3}$	$(7.04 \pm 0.08)10^{-3}$	$(5.53 \pm 0.05)10^{-3}$	$(7.02 \pm 0.09)10^{-3}$
13	$(3.73 \pm 0.03)10^{-3}$	$(6.63 \pm 0.08)10^{-3}$	$(5.32 \pm 0.05)10^{-3}$	$(6.96 \pm 0.09)10^{-3}$
14	$(3.45 \pm 0.03)10^{-3}$	$(6.35 \pm 0.07)10^{-3}$	$(5.22 \pm 0.05)10^{-3}$	$(6.52 \pm 0.08)10^{-3}$
15	$(3.18 \pm 0.03)10^{-3}$	$(6.30 \pm 0.07)10^{-3}$	$(4.94 \pm 0.05)10^{-3}$	$(5.93 \pm 0.08)10^{-3}$
16	$(2.91 \pm 0.03)10^{-3}$	$(5.95 \pm 0.07)10^{-3}$	$(4.25 \pm 0.04)10^{-3}$	$(4.50 \pm 0.07)10^{-3}$
17	$(2.21 \pm 0.02)10^{-3}$	$(5.47 \pm 0.07)10^{-3}$	$(2.79 \pm 0.04)10^{-3}$	$(2.18 \pm 0.05)10^{-3}$
18	$(1.44 \pm 0.02)10^{-3}$	$(4.39 \pm 0.06)10^{-3}$	$(1.52 \pm 0.03)10^{-3}$	$(1.31 \pm 0.04)10^{-3}$
19	$(7.27 \pm 0.14)10^{-4}$	$(3.01 \pm 0.05)10^{-3}$	$(5.46 \pm 0.16)10^{-4}$	
20	$(2.33 \pm 0.08)10^{-4}$	$(1.71 \pm 0.04)10^{-3}$		

At 1.6 GeV data were obtained using both the two- and four-state polarized deuteron beam. The vector-analyzing powers iT_{11} obtained from the four-state polarized beam are shown in Fig. 6 together with tensor analyzing powers T_{20} and T_{22}. The data for iT_{11} obtained with the two- and four-state beam are in good agreement and were averaged to make the fits. The values of iT_{11}, T_{20} and T_{22} averaged over θ are given in Table 4 together with the data obtained earlier at 1.8 GeV [5]. The tensor-analyzing powers T_{20} and T_{22} are very small at these high energies.

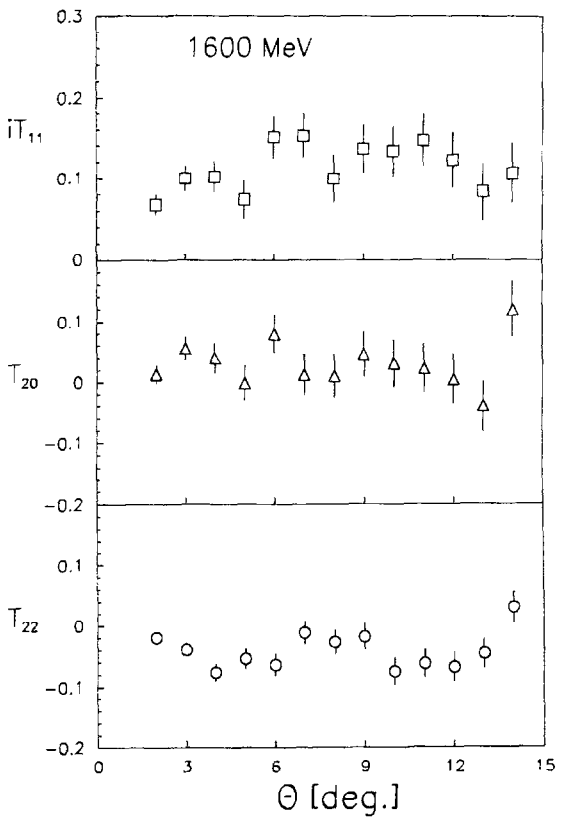

Fig. 6. Analyzing powers iT_{11}, T_{20}, T_{22} at 1.6 GeV.

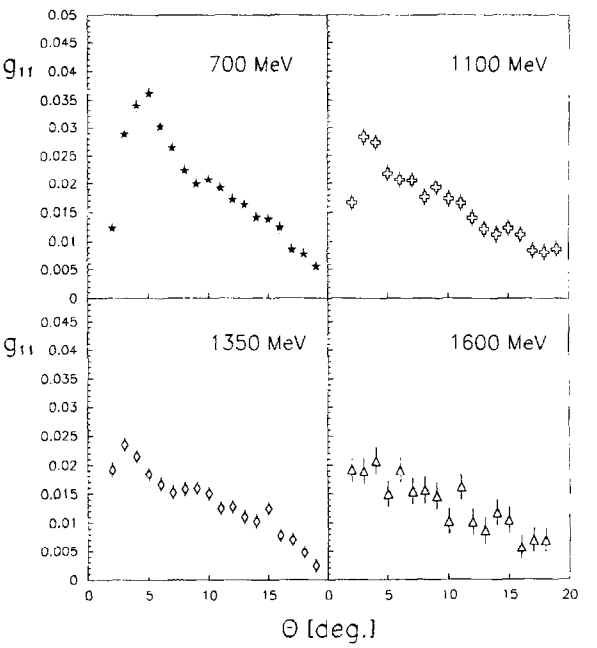

Fig. 7. Differential figure of merit g_{11} of the polarimeter at the four higher energies.

Table 4
Average analyzing powers for carbon analyzer, calculated at the scattering angle $\theta \geq 1.5°$ at 1.6 GeV from present calibration for four-state beam only and at 1.8 GeV from Ref. [5].

	1.6 GeV	1.8 GeV
$\langle iT_{11} \rangle$	0.10 ± 0.01	0.09 ± 0.01
$\langle T_{20} \rangle$	0.03 ± 0.01	-0.00 ± 0.01
$\langle T_{22} \rangle$	-0.04 ± 0.01	-0.03 ± 0.03

The differential figure of merit, $g_{11}(\theta)$, presented in Fig. 7 for the four energies, demonstrates that the most useful angular range is between 3° and 15°.

To calculate the integrated efficiency, figure of merit and averaged analyzing power we took the events with the scattering angle $\theta \geq 1.5°$. In Table 5 values of efficiency, figure of merit and average iT_{11} are given for the four energies, both as experimental values and values corrected for 100% track-reconstruction efficiency. The fraction of events having a scattering angle smaller than 1.5°, which are mostly due to multiple scattering, is $\sim 40\%$. These distributions are peaked at 1° and 0.5° for energies of 0.7 and 1.6 GeV, respectively.

POMME was previously calibrated at 0.7 GeV [4], using a 25.2 cm thick graphite analyzer and a 9 cm thick iron absorber placed in front of the Q counters. The vector-analyzing power and differential vector figure of merit of the previous and currents calibrations are compared in Fig. 8. The full symbols are the new results and the solid lines are the fit results of Ref. [4]. Both calibrations give a high figure of merit, $F_{11} \sim 0.07$ for the new, and ~ 0.05 for the previous calibration. Although the higher figure of merit obtained without iron corresponds to a reduced measurement time in an experiment using this polarimeter, the larger $\langle iT_{11} \rangle$ value obtained with iron will result in a smaller systematic error in polarization measurements. We conclude from these results that for deuteron energies higher than 0.7 GeV the use of an iron bloc is not necessary.

Table 5
Efficiency ε and figure of merit $\mathcal{F}_{11}$, corrected for 100% of track reconstruction, experimental efficiency ε^{exp}, figure of merit $\mathcal{F}_{11}^{exp}$, and averaged vector-analyzing power iT_{11} between $1.5^\circ \leqslant \theta \leqslant 20^\circ$

	ε	$\mathcal{F}_{11}$	ε^{exp}	$\mathcal{F}_{11}^{exp}$	$\langle iT_{11} \rangle$
0.7 GeV	0.426 ± 0.001	0.089 ± 0.002	0.245 ± 0.001	0.068 ± 0.001	0.12 ± 0.01
1.1 GeV	0.389 ± 0.001	0.074 ± 0.002	0.2243 ± 0.0005	0.0560 ± 0.0017	0.113 ± 0.01
1.35 GeV	0.357 ± 0.001	0.062 ± 0.002	0.2059 ± 0.0005	0.0472 ± 0.0015	0.10 ± 0.01
1.6 GeV	0.335 ± 0.001	0.059 ± 0.005	0.1889 ± 0.0005	0.0445 ± 0.0036	0.10 ± 0.01

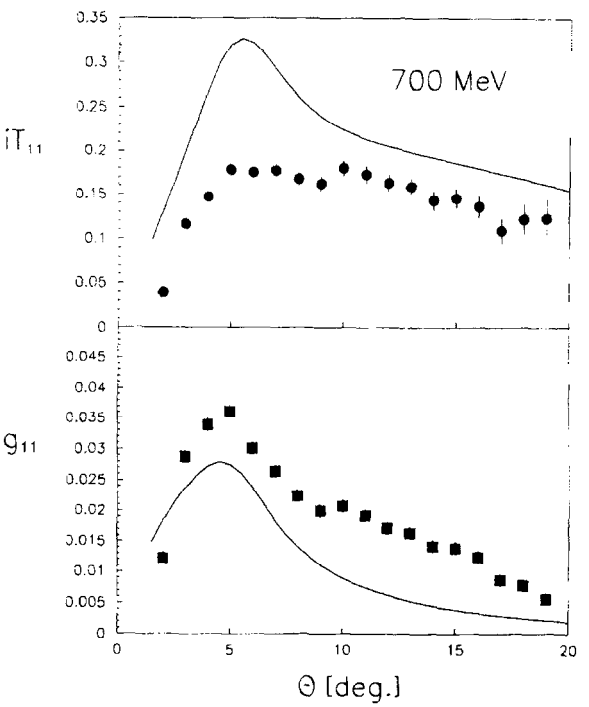

Fig. 8. Analyzing power iT_{11} and differential figure of merit g_{11} at 700 MeV from present calibration (points) and from Ref. [4] (lines).

5. Parametrization of the analyzing power iT_{11} and efficiency ε

Usually, an analytical parametrization of analyzing powers as a function of scattering angle and momentum is given, as it allows a quick estimation of counting rates, for experiments needing a polarimeter.

5.1. Parametrization of the low-energy data

The angular dependence of the analyzing power iT_{11} at the lower six energies were fitted with the same analytical function as in Ref. [4]:

$$iT_{11} = \frac{ax}{1 + bx^2 + cx^4} + d\,p_{mid} \sin 5\theta \exp\left[-\left(\frac{x-e}{f}\right)^2\right], \quad (8)$$

where the six parameters have a quadratic or linear dependence on $p' = p_{mid} - 2.4$ (where p_{mid} is the momentum of the deuteron at half the thickness of the analyzer) as follows:

$$a = a_0 + a_1 p' + a_2 p'^2,$$
$$b = b_0 + b_1 p' + b_2 p'^2,$$
$$c = c_0 + c_1 p' + c_2 p'^2,$$
$$d = d_0 + d_1 p',$$
$$e = e_0 + e_1 p',$$
$$f = f_0 + f_1 p', \quad (9)$$

with $x = p_{mid} \sin\theta$. In the fit we included all data from Ref. [4] with energies between 0.200 and 0.575 GeV.

In Fig. 9 the data from the previous calibration [4], for which a small-angle fast-rejection trigger was available, are shown as open circle; these data cover a larger θ range.

The results of the present fit are the solid lines in Fig. 9. The fit of Ref. [4] is shown as a dotted line in this figure. The values of the parameters are in Table 6.

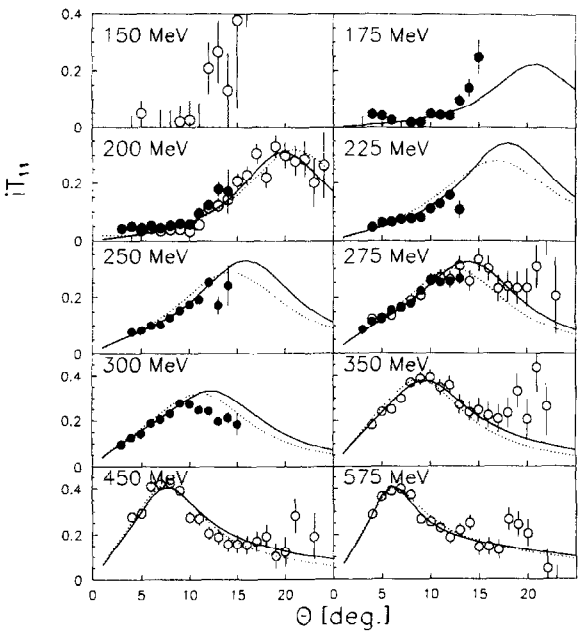

Fig. 9. Results of the low energy fit (solid line). The experimental values of the analyzing powers iT_{11} are shown as black circles. The open circles are the data from Ref.po1 and the dashed line is the fit of [4].

Table 6
The optimum values of the 15 parameters from the fit of iT_{11}, covering the low-energy data presented in this paper and the five lower energies from Ref. [3]

	0	1	2
a	-3.26 ± 0.70	5.81 ± 1.33	-1.83 ± 0.60
b	-97.0 ± 12.1	157.6 ± 19.0	-78.7 ± 8.3
c	$1836. \pm 359.$	$-3969. \pm 699.$	$2320. \pm 335.$
d	$90815. \pm 16165.$	$-46657 \pm 7705.$	
e	4.60 ± 0.35	-6.89 ± 0.17	
f	-1.66 ± 0.065	2.36 ± 0.106	

5.2. Parametrization of the high-energy data

The angular dependence of the analyzing powers are smooth at all the higher energies, and similar to what has been observed for proton–carbon analyzing powers [6,7]. Therefore, it seems resonable to use the same analytical formulae to fit the deuteron–carbon data, instead of using the fit from

Table 7
The optimum parameters for the six parameters from the fit of the inclusive deuteron–carbon vector analyzing power data

	0	1	2
a	1.1857 ± 0.0396	-0.8754 ± 0.0700	0.4721 ± 0.1360
b	3.1335 ± 0.0940	-1.1242 ± 0.1976	0.6191 ± 0.3581

Ref. [4], which requires a larger set of parameters. Furthermore, the function proposed in [7], which requires ten parameters, can be simplified without loss of fit quality, as follows:

$$iT_{11} = a\, x \exp(-bx), \tag{10}$$

with a form for a and b in Eq. (10) quadratic in p' (p' and x are defined as above) and requiring six parameters:

$$a = a_0 + a_1 p' + a_2 p'^2,$$
$$b = b_0 + b_1 p' + b_2 p'^2. \tag{11}$$

The results of these fits are shown in Fig. 10. A χ^2 of about 1 per degree of freedom was obtained for the four energies. The corresponding values of the six parameters are given in Table 7.

A parametrization of the polarimeter efficiency, $\varepsilon(\theta)$ as a function of scattering angle and incident momentum in the center of the carbon block has also been done; it is useful for counting-rate estimations and is also required to extract the polarization parameters from the global fit of $N(\theta, \phi)$ distributions, as discussed in Ref. [3]. The efficiency data, corrected for 100% track reconstruction in the chambers, were fitted with the following 17-parameter function:

$$\varepsilon = a \exp(-bx) + [c \exp(-ex) + d \exp(-fx)]x^g, \tag{12}$$

where x is as defined above and the coefficients a–g were parametrized as follows:

$$a = a_0 + a_1 p' + a_2 p'^2,$$
$$b = b_0 + b_1 p' + b_2 p'^2,$$
$$c = c_0 + c_1 p' + c_2 p'^2,$$
$$d = d_0 + d_1 p' + d_2 p'^2,$$

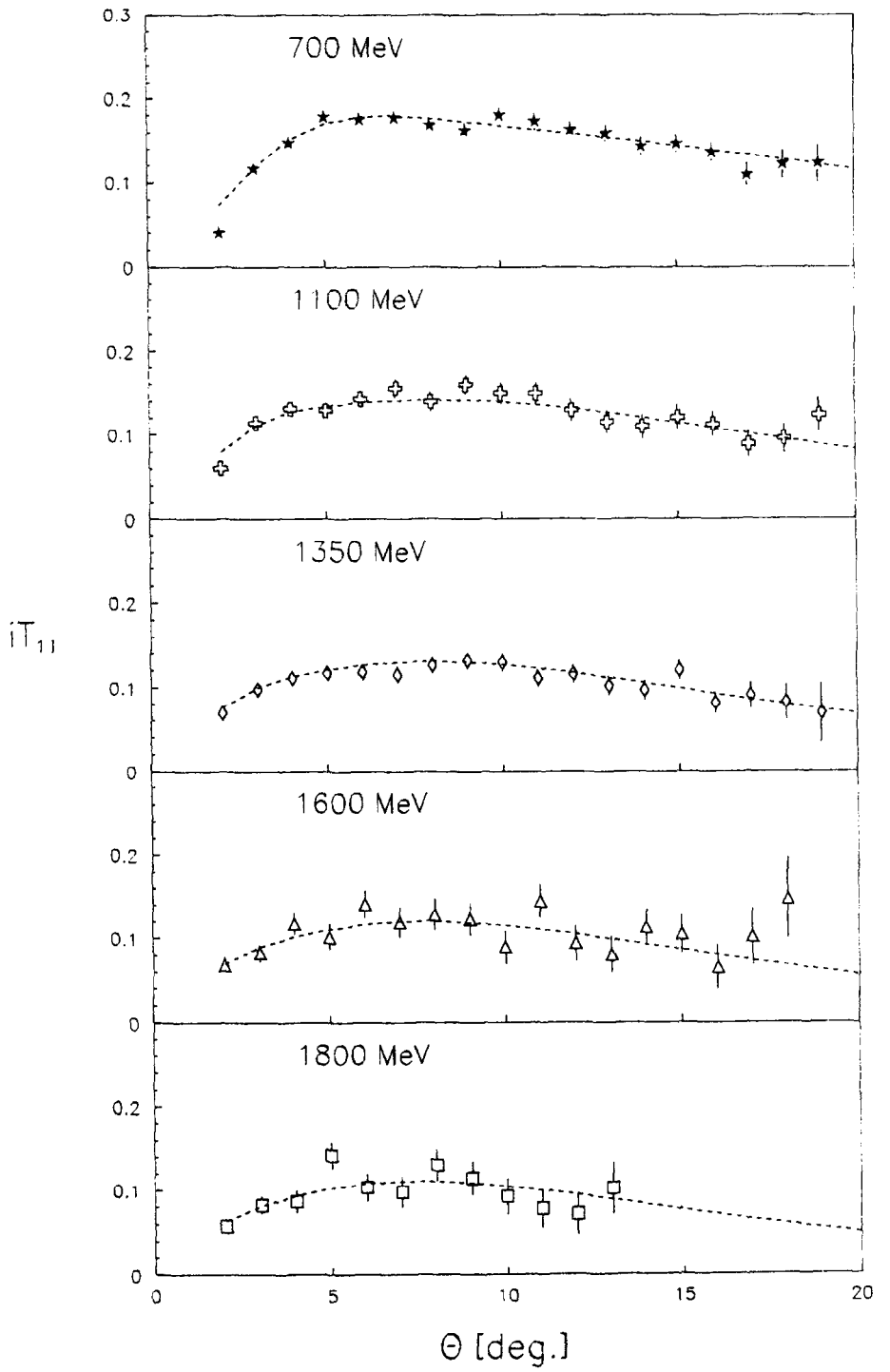

Fig. 10. Results of the six parameter fit (dotted lines) of the analyzing power iT_{11} for the four higher energies and the previous results from Ref. [5].

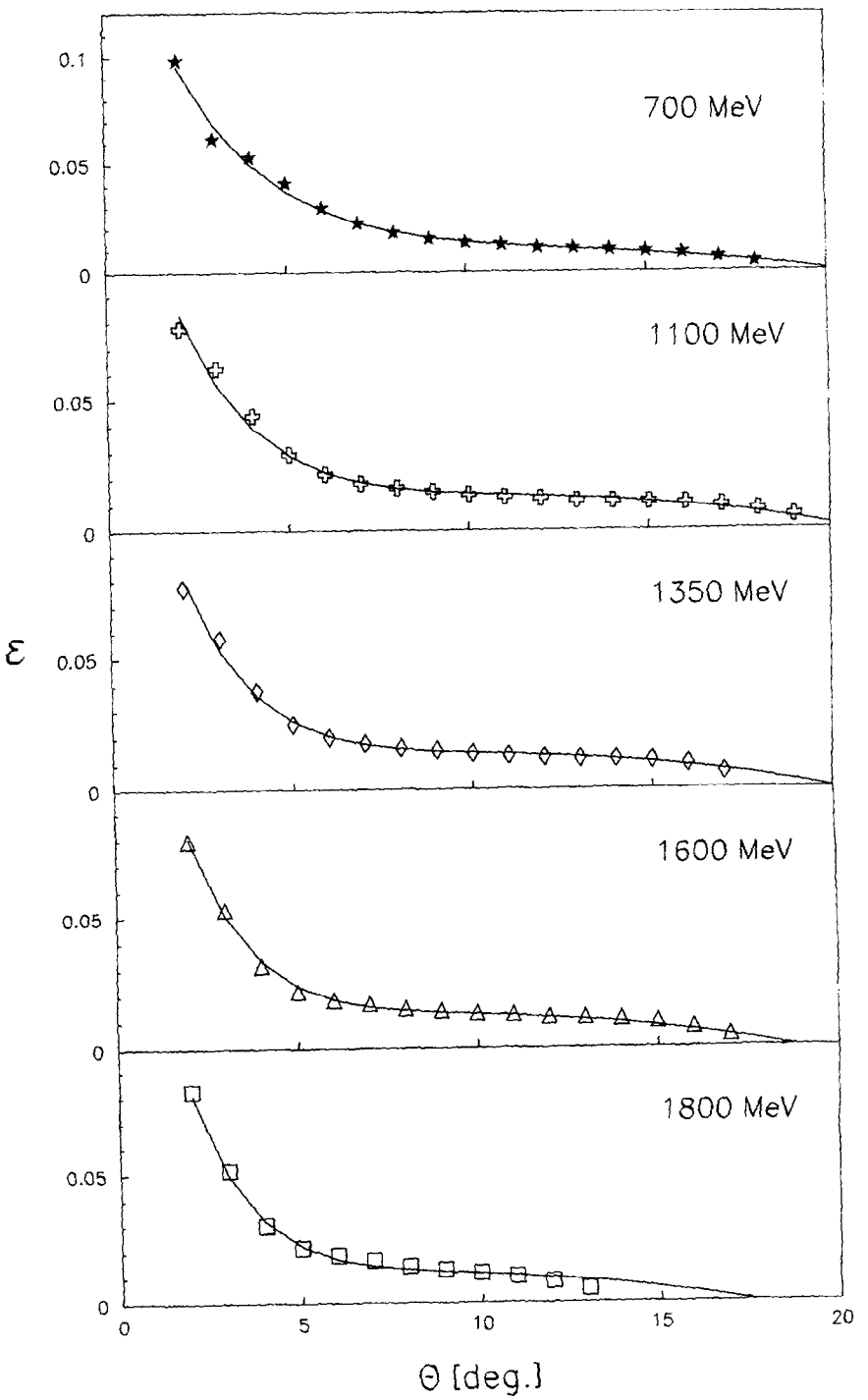

Fig. 11. Results of the seventeen parameter fit of the corrected efficiencies, ε, for the high energies

Table 8
The optimum parameters for the 17 parameters from the fit of the corrected efficiency of POMME

	0	1	2
a	0.1958 ± 0.0004	0.0362 ± 0.0008	0.0372 ± 0.0014
b	10.808 ± 0.012	− 1.202 ± 0.023	0.7421 ± 0.044
c	0.4398 ± 0.0001	0.0045 ± 0.0011	0.0872 ± 0.0022
d	− 0.3326 ± 0.0001	− 0.0184 ± 0.0010	− 0.0997 ± 0.0017
e	0.5668 ± 0.0001	0.3241 ± 0.0002	
f	0.2330 ± 0.0003	0.4844 ± 0.0012	
g	1.5364 ± 0.0005		

$$e = e_0 + e_1 p',$$

$$f = f_0 + f_1 p'$$

$$g = g_0. \tag{13}$$

The values of the seventeen parameters in Eq. (15) are given in Table 8 and the fits are shown in Fig. 11.

As was stressed in Section 3, the angular distributions of the differential efficiency depend on the geometrical acceptance of the polarimeter and on the beam conditions, and therefore depend upon the polarimeter geometry; the situation is different for the analyzing powers, which are quite independent of the polarimeter geometry.

6. Conclusions

We have presented the results of a new calibration of the 2π azimuthal acceptance polarimeter POMME, using vector-polarized deuterons, for deuteron kinetic energies in the range 0.175–0.300 GeV, and 0.700–1.6 GeV. The lower-energy data complement the previous calibration [4] by adding four energies within the range. The higher-energy data demonstrate that the effective vector-analyzing powers remain large. The results on vector analyzing power iT_{11} for energies between 0.175 and 0.300 GeV have been compared with the previous fit from Ref. [4] and a new global fit has been obtained. The data for energies between 0.7 and 1.8 GeV have been fitted with an analytical function depending on the deuteron-scattering angle and momentum. The present calibration, together with the previously published results, allows to extend the working range of POMME as a vector-deuteron polarimeter from 0.2 up to 1.8 GeV. This is especially interesting in anticipation of experiments where the polarization of deuteron emerging from a given reaction has to be measured in a wide range of energies, such as in the study of baryonic resonances excited in the reaction $(\vec{d}, \vec{d}')$ or in the $pp \to d\pi^+$ reaction. However, the tensor-analyzing powers are too small to be used to measure the tensor-deuteron polarization, in agreement with the conclusions of th e previous calibration [4]. Larger tensor-analyzing powers require use of an exclusive reaction, like d, p elastic scattering or d, 2p charge exchange [10]. A modified configuration of POMME has recently been tested [11] at Saturne. The fraction of d, p elastic-scattering events was enhanced by replacing the graphite target by a large liquid-hydrogen cell [12] and by adding a recoil protons detector. A prototype has been recently tested, showing large tensor- and vector-analyzing powers [13].

Acknowledgements

The authors would like to express their thanks to the Saturne technical services for help in installing this experiment and for providing very good beam conditions during the calibration.

References

[1] M. Morlet et al., Phys. Rev. C 46 (1992) 1008.
[2] B.N. Johnson et al., Phys. Rev. C 51 (1995) 1726.

[3] R. Abegg et al., contribution at Int. Symp. Deuteron-95, July 1995, Dubna, Russia.
[4] B. Bonin et al., Nucl. Instr. and Meth. A 288 (1991) 389.
[5] E. Tomasi-Gustafsson et al., Nucl. Instr. and Meth. A 366 (1995) 96.
[6] B. Bonin et al., Nucl. Instr. and Meth. A 288 (1991) 379.
[7] N.E. Cheung et al., Nucl. Instr. and Meth. A 363 (1995) 561.
[8] E. Grorud et al., Nucl. Instr. and Meth. A 288 (1990) 379.
[9] J. Arvieux et al., Nucl. Instr. and Meth. A 273 (1988) 48.
[10] S. Kox et al., Nucl. Instr. and Meth. A 346 (1994) 527.
[11] E. Tomasi-Gustafsson, J. Yonnet, V. Ladygine, Preprints LNS/Ph/94-07, LNS/Ph/95-13, CEN Saclay.
[12] L.B. Golovanov et al., Nucl. Instr. and Meth. A 381 (1996) 15.
[13] E. Tomasi-Gustafsson et al., in: C.E. Carlson, J. Domingo (Eds.), Proc. 14th Int. Conf. on Particles and Nuclei, World Scientific, 1997, p. 734.